A nanophotonic solar thermophotovoltaic device

DOI: 10.1038/nnano.2013.286
SOURCE: Lenert, Andrej, David M. Bierman, Youngsuk Nam, Walker R. Chan, Ivan Celanović, Marin Soljačić, and Evelyn N. Wang. "A Nanophotonic Solar Thermophotovoltaic Device." Nature Nanotechnology 9, no. 2, p. 126–130, 2014.

A Nanophotonic Solar Thermophotovoltaic Device

Andrej Lenert[a], David M. Bierman[a], Youngsuk Nam[a,d], Walker R. Chan[b,c], Ivan Celanović[c], Marin Soljačić[b,c] and Evelyn N. Wang[a,*]

[a]Device Research Laboratory
[b]Research Laboratory of Electronics
[c]Institute for Soldier Nanotechnology
Massachusetts Institute of Technology
Cambridge, MA, USA

[d]Department of Mechanical Engineering
Kyung Hee University, Yongin, Korea

Corresponding Author:
Evelyn N. Wang
Department of Mechanical Engineering
Massachusetts Institute of Technology
77 Massachusetts Avenue, 3-461B
Cambridge, MA 02139, USA
Tel: 1 (617) 324-3311
Email: enwang@mit.edu

DOI: 10.1038/nnano.2013.286
SOURCE: Lenert, Andrej, David M. Bierman, Youngsuk Nam, Walker R. Chan, Ivan Celanović, Marin Soljačić, and Evelyn N. Wang. "A Nanophotonic Solar Thermophotovoltaic Device." Nature Nanotechnology 9, no. 2, p. 126–130, 2014.

The most common approaches to generate power from sunlight are either photovoltaic (PV), in which sunlight directly excites electron-hole pairs in a semiconductor, or solar-thermal, in which sunlight drives a mechanical heat engine. Photovoltaic power generation is intermittent and typically only exploits a portion of the solar spectrum efficiently, whereas increased irreversibilities in smaller heat engines make the solar thermal approach best suited for utility-scale power plants. There is, therefore, an increasing need for hybrid technologies for solar power generation[1,2]. By converting sunlight into thermal emission tuned to energies directly above the photovoltaic bandgap using a hot absorber-emitter, solar thermophotovoltaics (STPVs) promise to leverage the benefits of both approaches: high-efficiency—by harnessing the entire solar spectrum[3-5]; scalability, compactness—because of their solid-state nature; and dispatchablility—in principle by storing energy using thermal or chemical means[6-8]. However, efficient collection of sunlight in the absorber and spectral control in the emitter are particularly challenging at high operating temperatures. This drawback has limited prior experimental demonstrations of this approach to conversion efficiencies around or below 1%[9-11]. Here we report on a full solar thermophotovoltaic device which, thanks to the nanophotonic properties of the absorber-emitter surface, reaches experimental efficiencies of 3.2%. The device integrates a multi-wall carbon nanotube absorber and a one-dimensional Si/SiO_2 photonic crystal emitter on the same substrate, with the absorber-emitter areas optimized to tune the energy balance. Our device is planar and compact and could become a viable option for high-performance solar thermophotovoltaic energy conversion.

DOI: 10.1038/nnano.2013.286
SOURCE: Lenert, Andrej, David M. Bierman, Youngsuk Nam, Walker R. Chan, Ivan Celanović, Marin Soljačić, and Evelyn N. Wang. "A Nanophotonic Solar Thermophotovoltaic Device." Nature Nanotechnology 9, no. 2, p. 126–130, 2014.

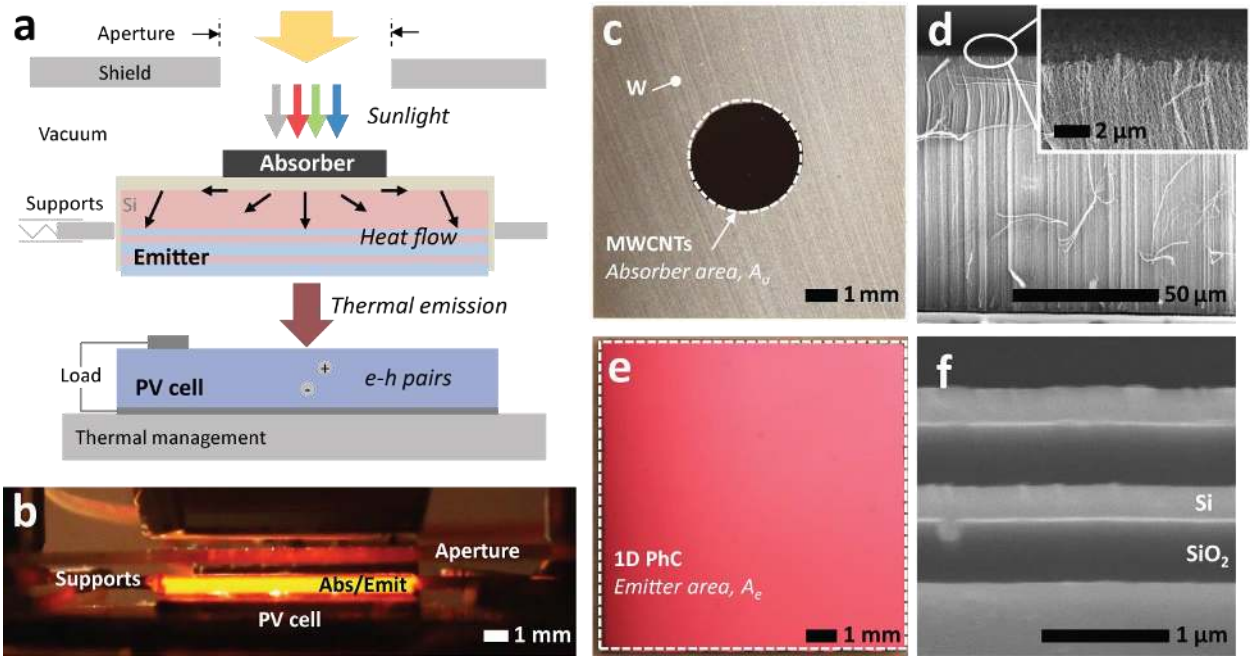

Figure 1 | Operating principle and components of the nanophotonic, area ratio optimized (NARO) STPV. Sunlight is converted to useful thermal emission, and ultimately electrical power, via a hot absorber-emitter. (**a**) Schematic and (**b**) optical image of our vacuum-enclosed devices composed of an aperture/radiation-shield, a array of multi-walled carbon nanotubes (MWCNT) as the absorber, a one-dimensional Si/SiO_2 photonic crystal emitter (1D PhC), a 0.55 eV bandgap PV cell (InGaAsSb[19-21]), and a chilled water cooling system. **c**, Absorber-side optical image of an $AR(=A_e/A_a)=10$ module showing spatially-defined MWCNTs (A_a=0.1 cm^2) on a W-coated Si substrate (1x1 cm planar area, 550 µm thick). **d**, SEM cross-section of the MWCNTs (inset: magnified view of the nanotube tips). **e**, Optical image of the 1D PhC emitter (A_e=1 cm^2). **f**, SEM cross-section of the 1D PhC showing the alternating layers of Si and SiO_2.

Because no portion of incident sunlight reaches the PV cell directly, the performance of STPVs relies on the efficiency of several intermediate energy conversion steps. Optically concentrated sunlight is converted into heat in the absorber; the absorber temperature rises; heat conducts to the emitter; the hot emitter thermally radiates towards the PV cell, where radiation is ultimately harnessed to excite charge carriers and generate power (Fig. 1a). The overall efficiency (η_{stpv}) can be expressed as a product of the optical efficiency of concentrating sunlight (η_o), the thermal efficiency of converting and

DOI: 10.1038/nnano.2013.286
SOURCE: Lenert, Andrej, David M. Bierman, Youngsuk Nam, Walker R. Chan, Ivan Celanović, Marin Soljačić, and Evelyn N. Wang. "A Nanophotonic Solar Thermophotovoltaic Device." Nature Nanotechnology 9, no. 2, p. 126–130, 2014.

delivering sunlight as heat to the emitter (η_t), and the efficiency of generating electrical power from the thermal emission (η_{tpv}):

$$\eta_{stpv} = \eta_o \eta_t \eta_{tpv} \tag{1}$$

The TPV efficiency (η_{tpv}) hinges on the spectral properties and the temperature of the emitter. A spectrally selective emitter should have high emittance for energies above the PV bandgap (E_g) and low emittance for energies below the bandgap. In order to excite enough thermal modes for substantial emission above the bandgap, the emitter temperature should ideally[12] be high enough such that Planck's blackbody peak approaches the bandgap, *i.e.,* by Wien's displacement law:

$$T_e^{opt} \approx 2336 \text{ [K/eV]} \cdot E_g \tag{2}$$

The high temperature operation of the emitter poses two key challenges to efficient STPV power conversion: collecting sunlight to efficiently reach T_e^{opt}, and maintaining spectral selectivity at elevated temperatures. Past STPV embodiments have relied on the intrinsic properties of materials such as tungsten[9,10]. For the absorber, one approach to effectively enhance the intrinsic solar absorptivity of materials is to use macro cavity geometries. Because of the high aspect ratio of the cavity needed to enhance absorption, this approach typically requires high levels of optical concentration to reach T_e^{opt} (*e.g.*, 3,183 times as used by Datas and Algora[9], 4,600 times as used by Vlasov *et al.*[10]). Such high optical concentration in turn requires complex systems with relatively low optical efficiencies (η_o~65%)[9]. For the emitter, the intrinsic spectral selectivity of tungsten is poor at T_e^{opt} since the emissivity at low photon energies ($< E_g$) increases with temperature, accompanying an increase in the electrical resistivity[13]. Ultimately, the reliance on the intrinsic spectral properties of materials for the absorber-emitter has limited previously reported experimental STPVs to conversion efficiencies around 1%[9-11].

To improve the performance of the absorber-emitter, researchers have investigated the design of structured surfaces[5,6,14-21] with spectral properties approaching those of ideal STPV components; specifically, the use of photonic crystals to control the photon density of states for narrow-band selective emission[5,6,14-20] . Simulation studies using

DOI: 10.1038/nnano.2013.286
SOURCE: Lenert, Andrej, David M. Bierman, Youngsuk Nam, Walker R. Chan, Ivan Celanović, Marin Soljačić, and Evelyn N. Wang. "A Nanophotonic Solar Thermophotovoltaic Device." Nature Nanotechnology 9, no. 2, p. 126–130, 2014.

realistic nanophotonic surfaces predict STPV efficiencies exceeding 40%[5,15,21]. Although the intrinsic material properties are sensitive to temperature, the surface structure affords a degree of spectral tunability which is temperature independent. Nevertheless, these surfaces have not yet been integrated into STPV devices operating at high enough temperatures for efficient power conversion.

In our device, the spectral properties of the absorber-emitter are tailored through surface nanostructuring in a compact planar layout (Fig. 1a,b) without resorting to more complex STPV configurations. The absorber-emitter module was composed of an array of multi-wall carbon nanotubes as the solar absorber and a one-dimensional Si/SiO_2 photonic crystal as the selective emitter. We varied the emitter-to-absorber area ratio ($AR=A_e/A_a$) from 1 to 10 to achieve optimal performance. With increasing area ratio, we supply enough heat for the absorber-emitter to reach T_e^{opt} by increasing the level of irradiance and leveraging the high absorptance of the nanotube array. Thermal resistance between the absorber and emitter is minimized by integrating the absorber and emitter on the same conductive silicon substrate such that heat is effectively delivered to the emitter via thermal spreading. Since the absorber area is reduced with respect to the planar area of the sample (Fig. 1c), the area for re-emissive losses from the nearly-blackbody nanotube array surface is decreased, thus boosting thermal efficiency. To reduce parasitic radiative losses, we metallized the sides of the silicon substrate and inactive area around the nanotube absorber with W, a relatively low-emissivity high-temperature material, and incorporated a high-reflectivity Ag-coated shield (Fig. 1a) to recycle this parasitic radiation back to the device.

Vertically-aligned carbon nanotubes were chosen as the solar absorber due to their high-temperature stability in vacuum and their nearly ideal absorptance, crucial for absorbing highly-concentrated irradiance at elevated emitter-to-absorber area ratios. As shown in Fig. 1d, the as-grown nanotubes are 10-15 nm in outer diameter and 80-100 μm tall with a ~0.5 μm variation in height at the tips. The broad-spectrum absorptance of the nanotube array in this study exceeds 0.99 (see SI: Absorber Characterization), consistent with previous reports for similar nanotube array geometries[22-24].

The multilayer Si/SiO_2 structure of the photonic crystal, composed of five alternating layers of Si and SiO_2 (Fig. 1e,f), improves the spectral matching between the emittance of the emitter and the internal quantum efficiency of the InGaAsSb PV cell[25-27] (E_g=0.55 eV). These materials were chosen for ease of fabrication and high-temperature compatibility with

DOI: 10.1038/nnano.2013.286
SOURCE: Lenert, Andrej, David M. Bierman, Youngsuk Nam, Walker R. Chan, Ivan Celanović, Marin Soljačić, and Evelyn N. Wang. "A Nanophotonic Solar Thermophotovoltaic Device." Nature Nanotechnology 9, no. 2, p. 126–130, 2014.

the silicon substrate. The layer thicknesses were optimized via a constrained global optimization of the product of efficiency and power density[6].

Our mechanical system ensured alignment and gap control while minimizing parasitic conduction losses (see SI: Experimental Setup). The entire experimental layout was maintained in vacuum (< 0.5 Pa) to suppress convective and conductive heat transfer through the environment. We used a Xe-arc light source to simulate the solar spectrum and to supply a range of irradiances (H_s) from 10 to 75 Wcm^{-2}.

To gain more insight into the complex energy conversion in our nanophotonic, area ratio optimized (NARO) STPV devices and compare it to theoretical predictions, we conducted two independent experiments—TPV and STPV. We investigated the maximum output power density (p_{out}) of the PV diode as a function of the absorber-emitter temperature (T_{ae}) in the TPV experiment and irradiance (H_s) in the STPV experiment. The temperature measurement in the TPV characterization was achieved by bonding a fine gage thermocouple directly to the absorber-side of the substrate.

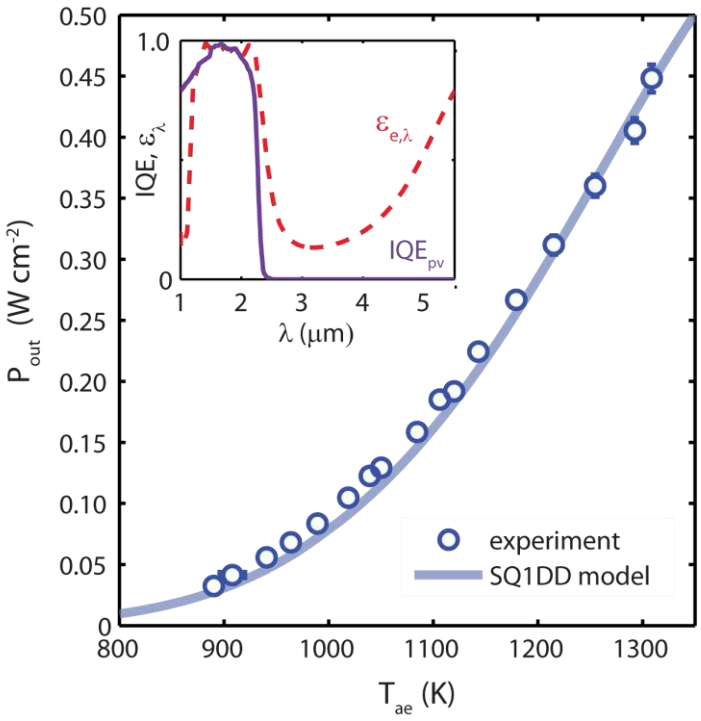

Figure 2 | TPV characterization. Electrical output power density (p_{out}) generated by the InGaAsSb PV cell as a function of the 1D Si/SiO_2 PhC emitter temperature. Inset depicts the measured[4] spectral emittance of the 1D PhC at 1285 K and

DOI: 10.1038/nnano.2013.286
SOURCE: Lenert, Andrej, David M. Bierman, Youngsuk Nam, Walker R. Chan, Ivan Celanović, Marin Soljačić, and Evelyn N. Wang. "A Nanophotonic Solar Thermophotovoltaic Device." Nature Nanotechnology 9, no. 2, p. 126–130, 2014.

the internal quantum efficiency of the PV used by the SQ1DD model. Model prediction (solid line) shows an excellent agreement with experimental points (markers). Error bars represent 95% confidence interval – see Methods.

As shown in Fig. 2, the output power of the PV cell is highly temperature-dependent as higher energy modes ($> E_g$) are excited with increasing emitter temperature. These experimental results are supported by a spectral quasi-1D diffuse radiative network model (SQ1DD). Our model assumes isothermal operation of the absorber-emitter (*i.e.*, $T_a=T_e=T_{ae}$) and accounts for the experimentally measured spectral properties of the components and the geometrical configuration of our planar STPV layout (see SI: Modeling). The results of the TPV experiment serve as validation of our model and provide an indirect method for determining the absorber-emitter temperature from the measured output power. This approach was used in the STPV characterization since a direct *in-situ* measurement of the absorber-emitter temperature increases parasitic losses and reduces the efficiency.

With the TPV performance characterized, we investigated the full energy conversion processes in our NARO-STPVs with increasing emitter-to-absorber area ratios. Fig. 3a shows the electrical output power of the STPV devices as a function of irradiance (H_s) and the absorber-emitter temperature (determined using the relation between p_{out} and T_{ae} shown in Fig. 2). The upper and lower estimates of our SQ1DD model (associated with treating H_s as collimated or diffuse, respectively) bound the data within the experimental uncertainty.

The effect of increasing area ratio is manifested in shifting the operating points to a regime of increased irradiance (H_s) relative to the thermal re-emission loss (σT_{ae}^4). If we consider the absorber solar collection efficiency (a major component of the thermal efficiency) for a blackbody surface:

$$\eta_a^{BB} = 1 - \frac{\sigma T_{ae}^4}{H_s} \tag{3}$$

we observe that decreasing the $\sigma T_{ae}^4/H_s$ ratio results in higher absorber efficiency. For our nearly-blackbody nanotube absorbers, this regime graphically corresponds to the lower right corner of Fig. 3a. Using equation (3), we estimated that the absorber efficiency for *AR* 10 is above 75%.

DOI: 10.1038/nnano.2013.286
SOURCE: Lenert, Andrej, David M. Bierman, Youngsuk Nam, Walker R. Chan, Ivan Celanović, Marin Soljačić, and Evelyn N. Wang. "A Nanophotonic Solar Thermophotovoltaic Device." Nature Nanotechnology 9, no. 2, p. 126–130, 2014.

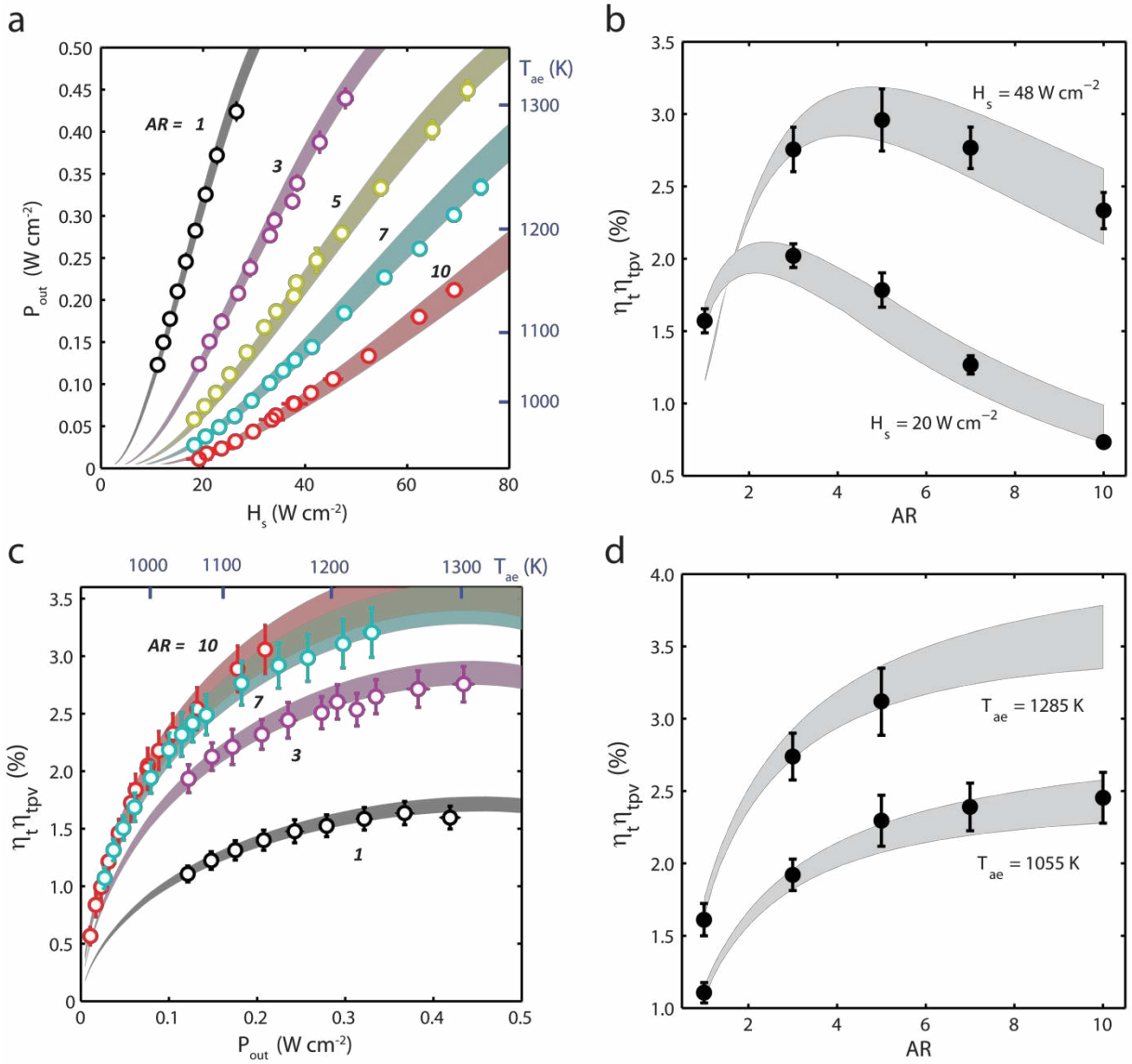

Figure 3 | Performance characterization and optimization of the nanophotonic STPV device. a, Electrical output power density (p_{out}) and absorber-emitter temperature (T_{ae} determined from Fig. 2) with increasing H_s (input solar power normalized by the aperture area) for AR=1 to 10. As the area ratio is increased, the device operates in a regime of decreased $\sigma T_{ae}^4/H_s$, which is favorable for the absorber efficiency of the nanotube array. **b,** Conversion efficiency (concentrated solar to electrical, $\eta_t\eta_{tpv}$) with increasing area ratio for a fixed H_s=20 and 48 W/cm^2. Competing effects of the thermal efficiency and the TPV efficiency lead to an optimal area ratio for a fixed H_s. **c,** Conversion efficiency as a function of the p_{out}, or equivalently, T_{ae} (AR=5 omitted for clarity). **d,** At a given p_{out} or T_{ae}, the conversion efficiency

DOI: 10.1038/nnano.2013.286
SOURCE: Lenert, Andrej, David M. Bierman, Youngsuk Nam, Walker R. Chan, Ivan Celanović, Marin Soljačić, and Evelyn N. Wang. "A Nanophotonic Solar Thermophotovoltaic Device." Nature Nanotechnology 9, no. 2, p. 126–130, 2014.

increases with increasing area ratio which is attributed to an increase in thermal efficiency. Markers are experimental points (error bars represent 95% confidence interval – see Methods); solid bands represent the SQ1DD model: treating H_s as collimated or diffuse sets the upper and lower bounds, respectively.

Nevertheless, absorber efficiency is only a component of the overall STPV efficiency. Indeed, the efficiency of converting concentrated sunlight into electrical power ($\eta_t\eta_{tpv}$) does not monotonically increase with increasing area ratio for a fixed irradiance (H_s); as shown in Fig. 3b, an optimal area ratio exists. To understand why this optimal area ratio arises, the competing effects of the thermal efficiency and the TPV efficiency are considered. The thermal efficiency is significantly enhanced as the area ratio is increased due to a rise in absorber efficiency (as explained above). In contrast, with increasing area ratio for a fixed H_s, the operating temperature of the absorber-emitter decreases since the ratio of the absorbed solar power ($\sim A_a H_s$) relative to the thermal emission ($\sim A_e \sigma T_{ae}^4$) decreases; ultimately leading to a decrease in TPV efficiency as the temperature drops significantly below the T_e^{opt}. These two competing effects lead to an optimal area ratio for a fixed irradiance, or equivalently, for a fixed optical concentration (10 times = 1 Wcm^{-2}, *ASTM E772*). In general, the optimum area ratio increases with optical concentration as shown in Fig. 3b, where the optimum shifts from approximately AR=2 to AR=5 as H_s is increased from 20 to 48 Wcm^{-2}.

Using the relation between p_{out} and T_{ae} (Fig. 2), we investigated the system performance as a function of absorber-emitter temperature. Fig. 3c shows that the efficiency initially increases sharply with emitter temperature (below 1200 K) as modes with energies above E_g are increasingly excited. As the temperature approaches T_e^{opt}, the efficiency plateaus as increasing useful emission (*i.e.*, radiation at $E > E_g$) is balanced by increasing re-emission losses and PV inefficiencies associated with high photocurrents. Increasing area ratio for a given absorber-emitter temperature results in increased conversion efficiency (Fig. 3d). Since the TPV efficiency is determined by the emitter temperature, the relative increase in conversion efficiency ($\eta_t\eta_{tpv}$) is completely attributed to the increase in thermal efficiency. At T_e^{opt} (1285 K), we experimentally demonstrated a two-fold increase in thermal efficiency from AR=1 to AR=5.

DOI: 10.1038/nnano.2013.286
SOURCE: Lenert, Andrej, David M. Bierman, Youngsuk Nam, Walker R. Chan, Ivan Celanović, Marin Soljačić, and Evelyn N. Wang. "A Nanophotonic Solar Thermophotovoltaic Device." Nature Nanotechnology 9, no. 2, p. 126–130, 2014.

Overall, the highest conversion efficiency ($\eta_t\eta_{tpv}$) that we measured is 3.2±0.2% using an AR=7 device, which is three times greater than previous STPV experiments[9]. This was achieved using a compact design at substantially lower levels of optical concentration (~750 times), which will enable higher optical efficiencies. As shown in Fig. 4, significant enhancements in efficiency relative to a gray body absorber-emitter (ε=0.5) were achieved through the use of: (i) a 1D Si/SiO_2 photonic crystal for improved spectral performance of the emitter and a vertically-aligned multi-walled carbon nanotube array for nearly ideal solar absorptance (a two-fold contribution to the improvement in $\eta_t\eta_{tpv}$) and (ii) optimization of the active emitter-to-absorber area ratio (an additional two-fold improvement). Optimizing area ratio at a fixed optical concentration with a nanophotonic absorber-emitter, experimentally demonstrated in this work, can be easily implemented in future STPV designs to increase overall efficiency.

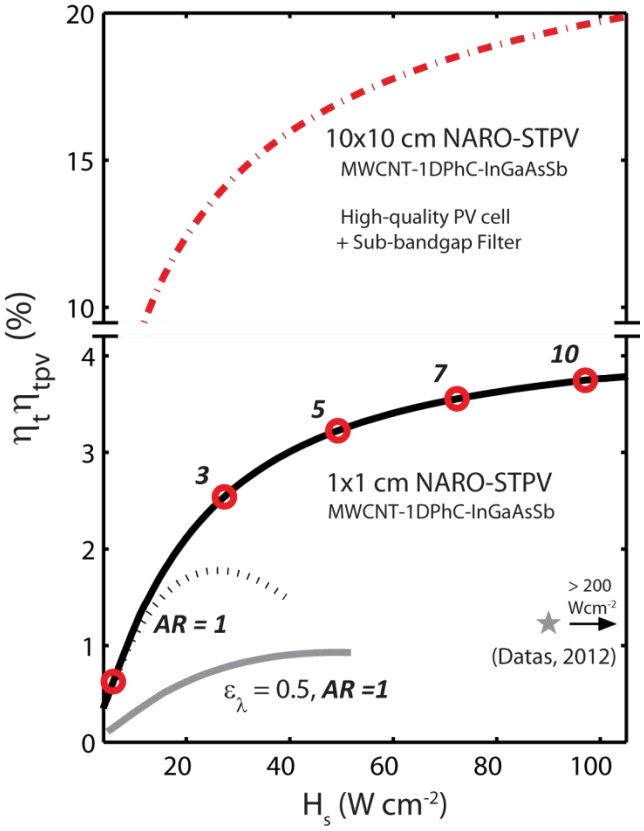

Figure 4 | Relative improvements in efficiency and near-term predictions for nanophotonic, area ratio optimized (NARO) STPVs. Conversion efficiency ($\eta_t\eta_{tpv}$) as function of a solar irradiance (H_s). Contributions to $\eta_t\eta_{tpv}$ relative to a gray body absorber-emitter: MWCNT-1DPhC absorber-emitter (two-fold improvement), area ratio optimization

DOI: 10.1038/nnano.2013.286
SOURCE: Lenert, Andrej, David M. Bierman, Youngsuk Nam, Walker R. Chan, Ivan Celanović, Marin Soljačić, and Evelyn N. Wang. "A Nanophotonic Solar Thermophotovoltaic Device." Nature Nanotechnology 9, no. 2, p. 126–130, 2014.

(additional two-fold improvement). Efficiencies approaching 20% were predicted with a scaled-up (10x10 cm) NARO-STPV utilizing a high-quality 0.55 eV PV module with a sub-bandgap reflector[20]. All points and predictions were made using the SQ1DD model (H_s was treated as collimated).

From the SQ1DD model, our highest efficiency operating point corresponds to a temperature of 1235 K with 54% thermal efficiency and 5.8% TPV efficiency. As the device scales in planar area from 1x1 cm to 10x10 cm (Fig. 4), the thermal efficiency will improve to ~75% as parasitic losses to the inactive area and mechanical supports decrease from 91% to 20% of the useful emission (see Fig. S5). Another important aspect limiting our conversion efficiency is the performance of the PV cell (V_{oc}=0.57E_g, 0.48 fill factor, 83% active area). Using an improved, yet realistic 0.55 eV InGaAsSb cell (V_{oc}=0.70E_g, 0.74 fill factor, 90% active area) and a sub-bandgap photon reflecting filter[26], the STPV efficiency will approach 20% at moderate optical concentrations (Fig. 4). Although this result requires scale up of our processing and experimental systems, our robust experimental STPV demonstration of the (1 cm^2) nanophotonic absorber-emitter and key design elements validates our model. The efficiency can be further enhanced through improvements in low-bandgap PVs (such as GaSb, Ge, and graphene-based PVs), better spectral control[5,15,21] and higher temperature operation. Unlike Si PV cells that have reached ~85% of their thermodynamic efficiency, the best-performing low-bandgap (TPV) cells exhibit 30-50% of their thermodynamic efficiency[10,25,26,28]. By re-optimizing the geometry of the 1D photonic crystal, our nanophotonic absorber-emitter may be paired with PV bandgaps up to ~0.7 eV; beyond this point, higher temperature photonic crystal materials are required, such as refractory metals[18]. The efficiency improvements demonstrated in this work, along with the promising predictions using a validated model, suggest the viability of nanophotonic STPVs for efficient and scalable solar energy conversion.

Methods

The absorber and the emitter were prepared using conventional physical and chemical vapor deposition (PVD, CVD) processes. The polycrystalline Si and SiO_2 layers of the 1D photonic crystal emitter was deposited by low-pressure and plasma-enhanced chemical vapor deposition, respectively[6]. The wafer was annealed after each deposition. On the back side of the emitter substrate, a 10 nm adhesion layer of Ti was sputtered, followed by a 200 nm W layer. Using a laser-cut

DOI: 10.1038/nnano.2013.286
SOURCE: Lenert, Andrej, David M. Bierman, Youngsuk Nam, Walker R. Chan, Ivan Celanović, Marin Soljačić, and Evelyn N. Wang. "A Nanophotonic Solar Thermophotovoltaic Device." Nature Nanotechnology 9, no. 2, p. 126–130, 2014.

acrylic contact mask, a seed layer for CNT growth was deposited onto the samples with electron-beam evaporation. The CNTs were grown using a high-temperature CVD process in a H_2/He environment by modifying a previously developed recipe[29]. The samples were heated to 720 ^oC from room temperature in ~10 mins and held at 720 ^oC for 5 mins to anneal the Fe seed. CNTs were grown for 10 mins at 720 ^oC using an ethylene gas carbon source. All of the flowing gases were preheated to 625 ^oC. Following the growth, the furnace was rapidly cooled in a H_2/He environment.

The absorber-emitter substrate was mechanically secured using a custom spring-loaded needle-support layout. Vacuum gaps of 400 μm and 300 μm separated the shield from the absorber and the emitter from the PV cell, respectively, such that the aperture/absorber and emitter/PV view factors exceeded 0.85. Manual linear stages were used to align and control the spacing between the reflecting shield, the absorber-emitter, and the PV cell. We conducted the experiments on each absorber-emitter pair at varying levels of flux of simulated solar radiation (H_s) through the aperture (10-75 Wcm^{-2}) by changing the distance between the light source and the experiment (see SI: Experimental Setup). H_s is defined as the input solar power through the aperture normalized by the aperture area, or equivalently, the nanotube absorber area. I-V and temperature measurements were obtained at steady operating conditions of the STPV device. Uncertainty in the reported experimental quantities was evaluated based on propagation of the following errors: variance (using a *t*-distribution with a 95% confidence interval), instrument error and resolution error. The PV temperature was maintained near 293 K using a chilled water loop (see Eq. S1).

Acknowledgments

This work is supported as part of the Solid-State Solar Thermal Energy Conversion (S3TEC) Center, an Energy Frontier Research Center funded by the U.S. Department of Energy, Office of Science, Office of Basic Energy Sciences under DE-FG02-09ER46577. A.L. acknowledges the support of the Martin Family Society, the MIT Energy Initiative and the National Science Foundation GRF. Y.N. acknowledges the support from Basic Science Research Program through the National Research Foundation of Korea (NRF) funded by the Ministry of Science, ICT & Future Planning (No. 2012R1A1A1014845). The authors thank Dr. C. Wang from Lincoln Laboratory for providing the InGaAsSb cells, H. Mutha, D. Li and Prof. C. V. Thompson's group (CNT growth); N. Miljkovic, T. Humplik, J. Sack, D. Preston and the

DOI: 10.1038/nnano.2013.286
SOURCE: Lenert, Andrej, David M. Bierman, Youngsuk Nam, Walker R. Chan, Ivan Celanović, Marin Soljačić, and Evelyn N. Wang. "A Nanophotonic Solar Thermophotovoltaic Device." Nature Nanotechnology 9, no. 2, p. 126–130, 2014.

Device Research Lab (SEMs, experimental setup); D. Kraemer, M. Luckyanova, Prof. G. Chen and the Nanoengineering group (advice).

Author Contributions

All authors contributed extensively to this work. A.L., D.M.B., and Y.N. envisioned and implemented the experimental study. A.L. and D.M.B. fabricated the absorber, executed the experiments, and wrote the paper. W.R.C. designed and fabricated the emitter. I.C., M.S. and E.N.W. supervised and guided the project.

Competing Financial Interests

The authors declare that they have no competing interests.

Additional Information

Supplementary information accompanies this paper at www.nature.com/naturenanotechnology. Reprints and permission information is available online at http://npg.nature.com/reprintsandpermissions/. Correspondence and requests for materials should be addressed to E.N.W. and A.L.

DOI: 10.1038/nnano.2013.286
SOURCE: Lenert, Andrej, David M. Bierman, Youngsuk Nam, Walker R. Chan, Ivan Celanović, Marin Soljačić, and Evelyn N. Wang. "A Nanophotonic Solar Thermophotovoltaic Device." Nature Nanotechnology 9, no. 2, p. 126–130, 2014.

References

1 J.W. Schwede *et al.* Photon-enhanced thermionic emission for solar concentrator systems. *Nat. Mater.* **9**, 762-767, (2010).
2 D. Kraemer *et al.* High-performance flat-panel solar thermoelectric generators with high thermal concentration. *Nat. Mater.* **10**, 532-538, (2011).
3 H. Nils-Peter & W. Peter. Theoretical limits of thermophotovoltaic solar energy conversion. *Semicond. Sci. Technol.* **18**, 151-156, (2003).
4 W. Shockley & H.J. Queisser. Detailed balance limit of efficiency of p-n junction solar cells. *J. Appl. Phys.* **32**, 510-519, (1961).
5 E. Rephaeli & S. Fan. Absorber and emitter for solar thermo-photovoltaic systems to achieve efficiency exceeding the Shockley-Queisser limit. *Opt. Express* **17**, 15145-15159, (2009).
6 W.R. Chan *et al.* Toward high-energy-density, high-efficiency, and moderate-temperature chip-scale thermophotovoltaics. *Proc. Acad. Nat. Sci. Phila.* **110**, 5309-5314, (2013).
7 A. Datas, D.L. Chubb & A. Veeraragavan. Steady state analysis of a storage integrated solar thermophotovoltaic (SISTPV) system. *Sol. Energ.* **96**, 33-45, (2013).
8 D.L. Chubb, B.S. Good & R.A. Lowe. Solar thermophotovoltaic (STPV) system with thermal energy storage. *AIP Conf. Proc.* **358**, 181-198, (1996).
9 A. Datas & C. Algora. Development and experimental evaluation of a complete solar thermophotovoltaic system. *Prog. Photovolt: Res. Appl.*, doi:10.1002/pip.2201 (2012).
10 A.S. Vlasov *et al.* TPV systems with solar powered tungsten emitters. *AIP Conf. Proc.* **890**, 327-334, (2007).
11 H. Yugami, H. Sai, K. Nakamura, N. Nakagawa & H. Ohtsubo. Solar thermophotovoltaic using Al2O3/Er3Al5O12 eutectic composite selective emitter. *IEEE Photovoltaic Spec. Conf.* **28**, 1214-1217, (2000).
12 D.L. Chubb. *Fundamentals of thermophotovoltaic energy conversion*. (Elsevier, Amsterdam, 2007).
13 R. Siegel & J.R. Howell. *Thermal radiation heat transfer*. (Hemisphere Pub. Corp., Washington, 1981).
14 M. Florescu *et al.* Improving solar cell efficiency using photonic band-gap materials. *Sol. Energ. Mat. Sol. C.* **91**, 1599-1610, (2007).
15 P. Bermel *et al.* Design and global optimization of high-efficiency thermophotovoltaic systems. *Opt. Express* **18**, A314-A334, (2010).
16 M. Ghebrebrhan *et al.* Tailoring thermal emission via Q matching of photonic crystal resonances. *Phys. Rev. A* **83**, 033810, (2011).
17 V. Rinnerbauer *et al.* Recent developments in high-temperature photonic crystals for energy conversion. *Energy Environ. Sci.* **5**, 8815-8823, (2012).
18 V. Rinnerbauer *et al.* High-temperature stability and selective thermal emission of polycrystalline tantalum photonic crystals. *Opt. Express* **21**, 11482-11491, (2013).
19 M. De Zoysa *et al.* Conversion of broadband to narrowband thermal emission through energy recycling. *Nat. Photon.* **6**, 535-539, (2012).
20 I. Celanovic, N. Jovanovic & J. Kassakian. Two-dimensional tungsten photonic crystals as selective thermal emitters. *Appl. Phys. Lett.* **92**, 193101-193103, (2008).
21 C. Wu *et al.* Metamaterial-based integrated plasmonic absorber/emitter for solar thermo-photovoltaic systems. *J. Opt.* **14**, 024005, (2012).
22 Z.-P. Yang, L. Ci, J.A. Bur, S.-Y. Lin & P.M. Ajayan. Experimental observation of an extremely dark material made by a low-density nanotube array. *Nano Lett.* **8**, 446-451, (2008).
23 Z.-P. Yang *et al.* Experimental observation of extremely weak optical scattering from an interlocking carbon nanotube array. *Appl. Opt.* **50**, 1850-1855, (2011).
24 H. Shi, J.G. Ok, H.W. Baac & L.J. Guo. Low density carbon nanotube forest as an index-matched and near perfect absorption coating. *Appl. Phys. Lett.* **99**, 211103-211106, (2011).
25 C.A. Wang *et al.* High-quantum-efficiency 0.5 eV GaInAsSb/GaSb thermophotovoltaic devices. *Appl. Phys. Lett.* **75**, 1305-1307, (1999).
26 M.W. Dashiell *et al.* Quaternary InGaAsSb thermophotovoltaic diodes. *IEEE Trans. Electron.* **53**, 2879-2891, (2006).
27 W. Chan *et al.* Modeling low-bandgap thermophotovoltaic diodes for high-efficiency portable power generators. *Sol. Energ. Mat. Sol. C.* **94**, 509-514, (2010).
28 N.E. Posthuma, J. van der Heide, G. Flamand & J. Poortmans. Emitter formation and contact realization by diffusion for germanium photovoltaic gevices. *IEEE Trans. Electron.* **54**, 1210-1215, (2007).

DOI: 10.1038/nnano.2013.286
SOURCE: Lenert, Andrej, David M. Bierman, Youngsuk Nam, Walker R. Chan, Ivan Celanović, Marin Soljačić, and Evelyn N. Wang. "A Nanophotonic Solar Thermophotovoltaic Device." Nature Nanotechnology 9, no. 2, p. 126–130, 2014.

29 G.D. Nessim *et al.* Low temperature synthesis of vertically aligned carbon nanotubes with electrical contact to metallic substrates enabled by thermal decomposition of the carbon feedstock. *Nano Lett.* **9**, 3398-3405, (2009).

DOI: 10.1038/nnano.2013.286
SOURCE: Lenert, Andrej, David M. Bierman, Youngsuk Nam, Walker R. Chan, Ivan Celanović, Marin Soljačić, and Evelyn N. Wang. "A Nanophotonic Solar Thermophotovoltaic Device." Nature Nanotechnology 9, no. 2, p. 126–130, 2014.

A Nanophotonic Solar Thermophotovoltaic Device

Andrej Lenert, David M. Bierman, Youngsuk Nam, Walker R. Chan, Ivan Celanović, Marin Soljačić and Evelyn N. Wang*

Corresponding author: enwang@mit.edu

This supplement contains:

DOI: 10.1038/nnano.2013.286
SOURCE: Lenert, Andrej, David M. Bierman, Youngsuk Nam, Walker R. Chan, Ivan Celanović, Marin Soljačić, and Evelyn N. Wang. "A Nanophotonic Solar Thermophotovoltaic Device." Nature Nanotechnology 9, no. 2, p. 126–130, 2014.

Absorber Characterization

MWNT Absorber Optical Characterization

The radiative properties of the MWNT absorbers were characterized across a broad range of wavelengths (Supplementary Fig. 1). Total reflectance (diffuse + specular) was gathered between 250 and 1750 nm using a UV-Vis-NIR spectrophotometer (*500i, Cary*) with a diffuse reflectance accessory. The baseline reference measurement was performed with a certified reflectance standard (*SRS-99-010*, *Labsphere*). The MWNT surface was further characterized in the infrared region (2.8-10 μm) using a FTIR (*Spectrum ONE, Perkin Elmer*). During these measurements, specular reflectance was measured at an incidence angle of 30 degrees using a variable angle specular reflection accessory (*VeeMax II*). Both characterizations support previously reported broadband emittance measurements exceeding 0.99[1-3]. Significant variations in emittance before and after high-temperature operation and amongst samples (*AR*=1 to 10) were not observed.

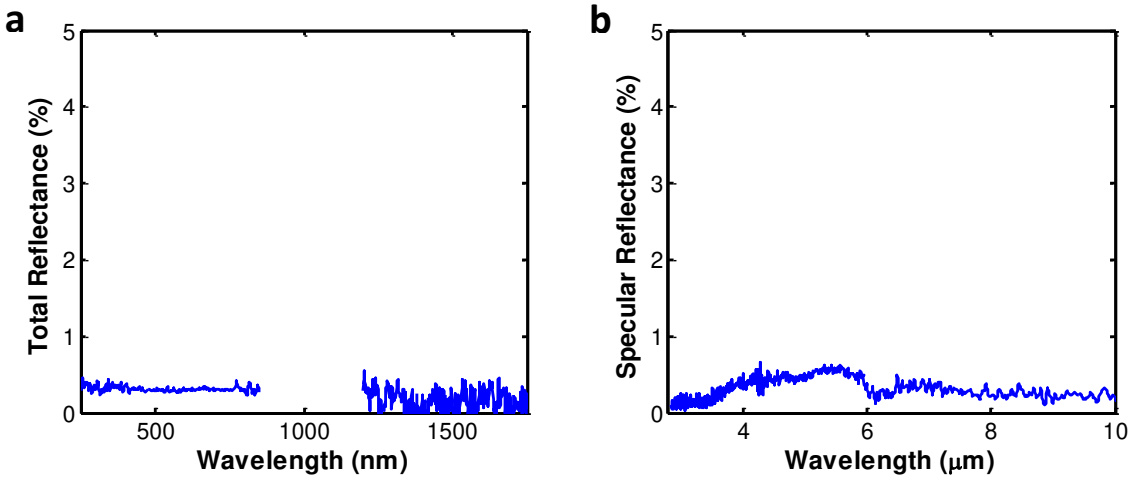

Supplementary Fig. 1 | Optical characterization of MWNT absorber. a, Total reflectance (diffuse + specular) spanning the relevant solar wavelength range (0.25-1.75 μm); data near 1 μm omitted due to high noise level associated with lamp/detector change. **b,** Specular reflectance (30° incident angle) in the infrared (2.8-10 μm).

DOI: 10.1038/nnano.2013.286
SOURCE: Lenert, Andrej, David M. Bierman, Youngsuk Nam, Walker R. Chan, Ivan Celanović, Marin Soljačić, and Evelyn N. Wang. "A Nanophotonic Solar Thermophotovoltaic Device." Nature Nanotechnology 9, no. 2, p. 126–130, 2014.

Visualization of Absorber-side Interfaces

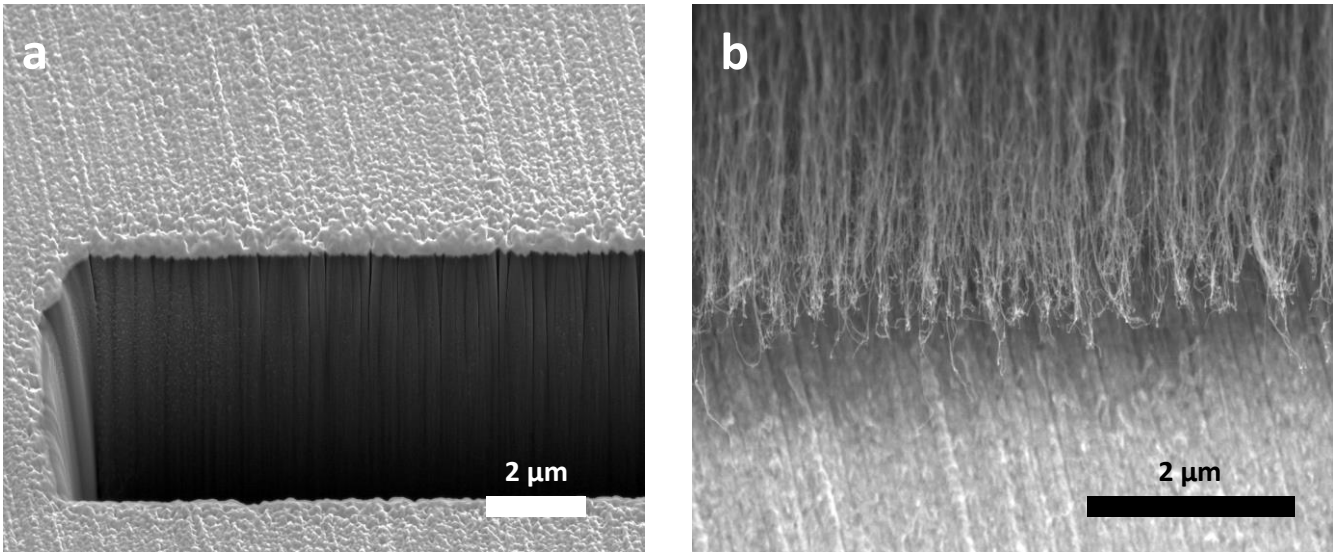

Supplementary Fig. 2 | SEMs of absorber-side interfaces: **a,** W/substrate and **b,** CNT/W.

Supplementary Fig. 2 shows the W/substrate and CNT/W absorber-side interfaces. These SEMs were taken on a sample after approximately 1 hr of high-temperature operation (1000-1300 K). The micro/nanoscale morphologies of the interfaces between the different materials are clearly distinguishable in the SEMs.

Experimental Set-up

Solar Simulator Calibration

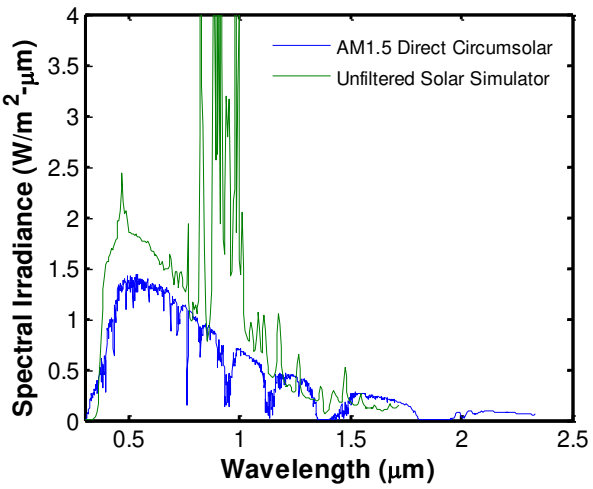

DOI: 10.1038/nnano.2013.286
SOURCE: Lenert, Andrej, David M. Bierman, Youngsuk Nam, Walker R. Chan, Ivan Celanović, Marin Soljačić, and Evelyn N. Wang. "A Nanophotonic Solar Thermophotovoltaic Device." Nature Nanotechnology 9, no. 2, p. 126–130, 2014.

Supplementary Fig. 3 | Simulated solar spectrum. Comparison between the AM1.5 direct spectrum used a standard for CSP applications and the spectrum provided by the Xe-arc lamp in our experiments.

The input power in our experiments was provided by a solar simulator (*92192, Newport Oriel Inc*.). While the Xe-arc spectrum deviates slightly from the standard AM1.5D (Supplementary Fig. 3), the MWNT absorbing surface displays broad-spectrum near-blackbody absorptance[1-3] (see Supplementary Fig. 1) such that the difference in spectrally-weighted absorptance for the two spectra is negligible.

Light from the solar simulator was concentrated using a focusing lens system (*Hi Flux Concentrator, Newport Oriel Inc*.), shown in Supplementary Fig. 4a. The concentrator has two distinct configurations, converging-diverging and converging, which enable a wide range of irradiances to be supplied. This light was further concentrated with a secondary concentrator—a converging "light pipe" which reduces the size of the illuminated spot. The "light pipe" was constructed by sputtering a 250 nm silver layer on large glass microscope slides. The slides were cut using a die saw and assembled into a square frustum. The input power was determined shortly after each experiment by measuring the power through the aperture used in the experiment. This value was obtained using a thermopile detector (*919P-040-50, Newport Oriel Inc*.), which measures the total radiative power incident on the sensing surface. To determine the irradiance, this power was normalized by the area of the aperture (or equivalently, the absorber area in our experiments). The irradiance was varied between 10 and 75 W/cm^2 by utilizing both optical configurations mentioned above and moving the optical setup relative to our vacuum-enclosed experimental setup (Supplementary Fig. 4b) along a linear track (*i.e.*, the farther the light source, the lower the irradiance).

DOI: 10.1038/nnano.2013.286
SOURCE: Lenert, Andrej, David M. Bierman, Youngsuk Nam, Walker R. Chan, Ivan Celanović, Marin Soljačić, and Evelyn N. Wang. "A Nanophotonic Solar Thermophotovoltaic Device." Nature Nanotechnology 9, no. 2, p. 126–130, 2014.

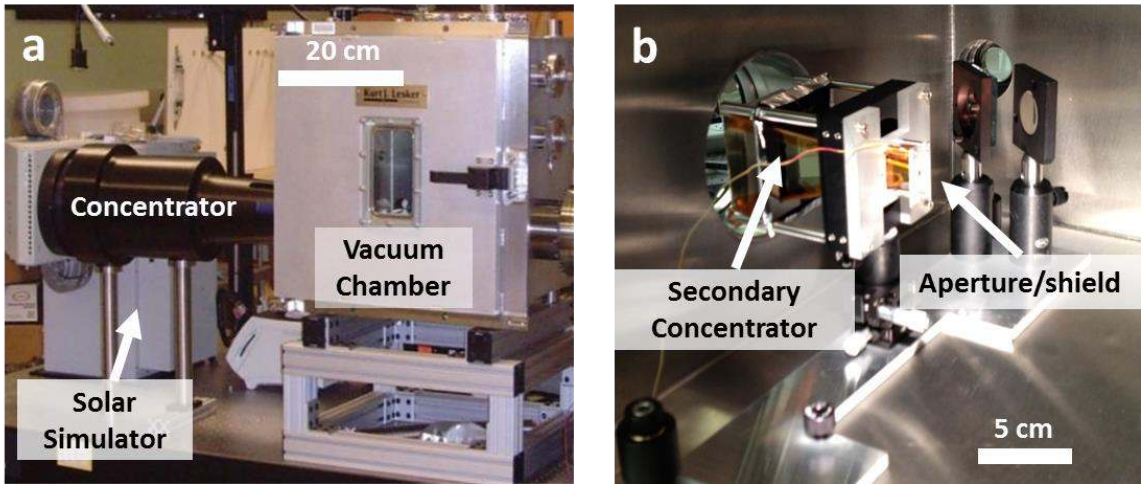

Supplementary Fig. 4 | Experimental setup. a, Optical image showing solar simulator, primary concentrator, and vacuum chamber. **b,** Optical image of the experimental setup inside the vacuum chamber showing the secondary concentrator and the aperture/shield assembly.

Alignment and Gap Control

We developed a mechanical system and procedure to ensure repeatable alignment and gap control between the absorber-emitter sample, the PV cell, and the aperture/shield. In a horizontal orientation as shown in Fig. 1a (with gravity pointing down), the PV cell assembly was first mounted to the thermal management stage which was fixed to a z-axis stage (*122-0101, Opto Sigma Corp.*). The absorber-emitter sample was then placed on top of the PV; since the PV and the emitter have equal dimensions, the sample edges were easily aligned with the PV edges using a vertical straightedge. Second, the mechanical support needles were brought into contact with two sides of the absorber-emitter (550 μm thickness) to secure its position while maintaining alignment with the PV cell. Three stainless steel mechanical supports were used in the design: two hypodermic needles (*27Gx1.25", B-D*) on one side and a spring-loaded pin (*POGO-72U-S, ECT*) on the opposite side. The spring-loaded pin ensured that a light force was constantly applied on the absorber-emitter and the supports, minimizing pitch errors due to thermal expansion of the sample during operation. After securing the sample, a 300 μm gap between the emitter and the PV cell was set using the z-stage to lower the PV cell assembly with respect to the mounted absorber-emitter. The experimental setup was then mounted in the vacuum chamber and aligned with the aperture/shield (Ag-coated) using a manual linear stage to set the gap. Finally, the setup was connected to the chilled water loop and the instrumentation via feedthroughs.

DOI: 10.1038/nnano.2013.286
SOURCE: Lenert, Andrej, David M. Bierman, Youngsuk Nam, Walker R. Chan, Ivan Celanović, Marin Soljačić, and Evelyn N. Wang. "A Nanophotonic Solar Thermophotovoltaic Device." Nature Nanotechnology 9, no. 2, p. 126–130, 2014.

TPV Emitter Temperature Measurement

The temperature of the absorber-emitter during the TPV-validation experiment was measured using a fine gage special limits thermocouple (*CHAL-005, Omega Engineering Inc.*) bonded to the absorber-side of the sample. The bond was established using a zirconia-based ceramic epoxy (*516 Ultra-Temp, Aremco Products Inc.*); the manufacturer's thermal annealing instructions were followed but in an inert (N_2/H_2-5%) environment to avoid oxidation of the MWNT absorber.

PV Temperature and Thermal Load

The temperature of the PV cell was measured using a type-K thermocouple (*Omega Engineering Inc.*) sandwiched between the packaged cell assembly and the thermal management stage. Chilled water was supplied to the thermal management stage using a liquid to liquid heat exchanger (*013736, NESLAB*) at a steady flow rate of 0.20±0.04 LPM and an inlet temperature of 291±0.4 K. In the range of our experiments results, the temperature of the PV cell (T_{pv}) was dependent on the output power density (p_{out}) according to the following line of best fit:

$$T_{pv}[K] = 291.8 + 6.59\, p_{out}[Wcm^{-2}] \quad \text{(S1)}$$

During our experiments, T_{pv} did not exceed 296 K. Using the flow rate and temperature measurements at the inlet and outlet of the stage, we determined the thermal load on the PV cell during operation:

$$q_{th}\,[Wcm^{-2}] = 0.33 + 15.46\, p_{out}\,[Wcm^{-2}] \quad \text{(S2)}$$

The above thermal load is specific to the TPV components and geometrical configuration used in our experimental setup. By combining the above information, we can extract an effective thermal resistance between the PV cell and the environment (the chilled water inlet in our case):

$$R_{eff} = \frac{T_{pv} - T_{in}}{q_{th}} = 0.404[KW^{-1}cm^2] \quad \text{(S3)}$$

Although our system relies on forced liquid convection to provide the desired experiment control, the above thermal resistance can easily be achieved using air-cooled heat sinks in a practical terrestrial application.

DOI: 10.1038/nnano.2013.286
SOURCE: Lenert, Andrej, David M. Bierman, Youngsuk Nam, Walker R. Chan, Ivan Celanović, Marin Soljačić, and Evelyn N. Wang. "A Nanophotonic Solar Thermophotovoltaic Device." Nature Nanotechnology 9, no. 2, p. 126–130, 2014.

Determining Maximum Power Output

We performed several current-voltage (I-V) sweeps using a precision source-meter (*2440, Keithley Instruments Inc.*) once steady state operation of the STPV device was established. The I-V sweep was conducted in a 4-wire configuration with 50 points acquired in the range of 0-0.7 V. The reported output power density (p_{out}) is an average of the maximum power points for each I-V sweep acquired at steady operating conditions, normalized by the total cell area (1 cm^2).

Modelling

We have developed a system level model to predict both input and output power to the device for a given equilibrium temperature. Our assumption of isothermal operation (quasi 1-D) is justified due to the geometry of the planar absorber/emitter device as well as its relatively high thermal conductivity (as supported by a highly-fidelity 2-D model[4]). When an equilibrium temperature is specified, heat transfer (radiation and conduction) with the surrounding components (PV cell, shield, supports, and vacuum chamber) can be determined. Radiative transfer is solved on a spectral basis through an energy balance at each surface. The spectral radiosity (J_λ) is the sum of the thermal emission ($E_{b\lambda}$) and the reflection of the irradiance (H_λ). The irradiance is defined as the portion of the radiosity from other surfaces (j) in the network which is intercepted by the surface of interest (i). The intercepted portion is determined using diffuse view factors (F_{ij}).

$$J_{\lambda_i} = \varepsilon_{\lambda_i} \mathrm{E}_{\mathrm{b}\lambda_i} + \left(1 - \varepsilon_{\lambda_i}\right) H_{\lambda_i} \tag{S4}$$

$$H_{\lambda_i} = \sum_{j=1}^{n} J_{\lambda_j} F_{ij} \tag{S5}$$

Equations S4 and S5 are solved for each surface at each wavelength. After integrating over all wavelengths, the total radiative heat transfer to each component is known.

Conduction from the supports is estimated using a fin approximation. This is justified by a small Biot number (<<0.1). For a fin with an adiabatic tip, the heat loss is given by the following equation:

$$\dot{q}_{fin} = (\mathrm{T_b} - \mathrm{T_v})\sqrt{\mathrm{h}\, P\, \mathrm{k}\, \mathrm{A}_c}\, \tanh(mL) \tag{S6}$$

DOI: 10.1038/nnano.2013.286
SOURCE: Lenert, Andrej, David M. Bierman, Youngsuk Nam, Walker R. Chan, Ivan Celanović, Marin Soljačić, and Evelyn N. Wang. "A Nanophotonic Solar Thermophotovoltaic Device." Nature Nanotechnology 9, no. 2, p. 126–130, 2014.

where T_b is the temperature at the contact between the absorber-emitter and the support, T_v is the temperature of the vacuum chamber, $\bar{h}$ is the average heat transfer coefficient (approximated using a linearized radiation coefficient), P is the perimeter, k is the thermal conductivity, A_c is the cross-sectional area, and L is the length of the support. The fin constant (mL) is given by:

$$mL = \sqrt{\frac{P\,\bar{h}}{k\,A_c}}L \tag{S7}$$

The emittance and the thermal conductivity for stainless steel (SS304) are estimated at the mean temperature of the fin.

The sum of the radiative emission and heat conduction is the total heat that must be supplied to the absorber-emitter to maintain the specified equilibrium temperature. From this energy balance, we solved for the required irradiance (H_s) based on two limiting cases: treating H_s as collimated or diffuse. For the collimated approximation, all of the incoming light through the aperture is simply incident on the MWNT absorber. For the diffuse approximation, the radiative flux passing through the aperture is split between the active MWNT absorber and the surrounding tungsten area based on their respective view factors (undergoing multiple reflections with the aperture/shield).

To determine the output power, we first solved for the total radiative heat transfer from the emitter to the PV cell for wavelengths smaller than that associated with the bandgap energy of the InGaAsSb cell (< 2.22 μm). This useful radiation generates photocurrent (I_{ph}) based on the following expression:

$$I_{ph} = \frac{-e}{hc_0}A_{pv}\int_0^\infty \lambda\, IQE_\lambda\, Q_{\lambda,e-pv}d\lambda \tag{S8}$$

where e is the charge of an electron, h is Planck's constant, c_0 is the speed of light in a vacuum, A_{pv} is the area of the PV cell, IQE_λ is the spectral internal quantum efficiency of the PV cell, and $Q_{\lambda,e\text{-}pv}$ is the spectral absorber radiation on the cell. Once the photocurrent was determined, the I-V characteristics (*i.e.*, maximum power point) of the PV cell were determined semi-empirically following the methods described by Chan *et al.*[5].

Power Conversion and Loss Mechanisms

DOI: 10.1038/nnano.2013.286
SOURCE: Lenert, Andrej, David M. Bierman, Youngsuk Nam, Walker R. Chan, Ivan Celanović, Marin Soljačić, and Evelyn N. Wang. "A Nanophotonic Solar Thermophotovoltaic Device." Nature Nanotechnology 9, no. 2, p. 126–130, 2014.

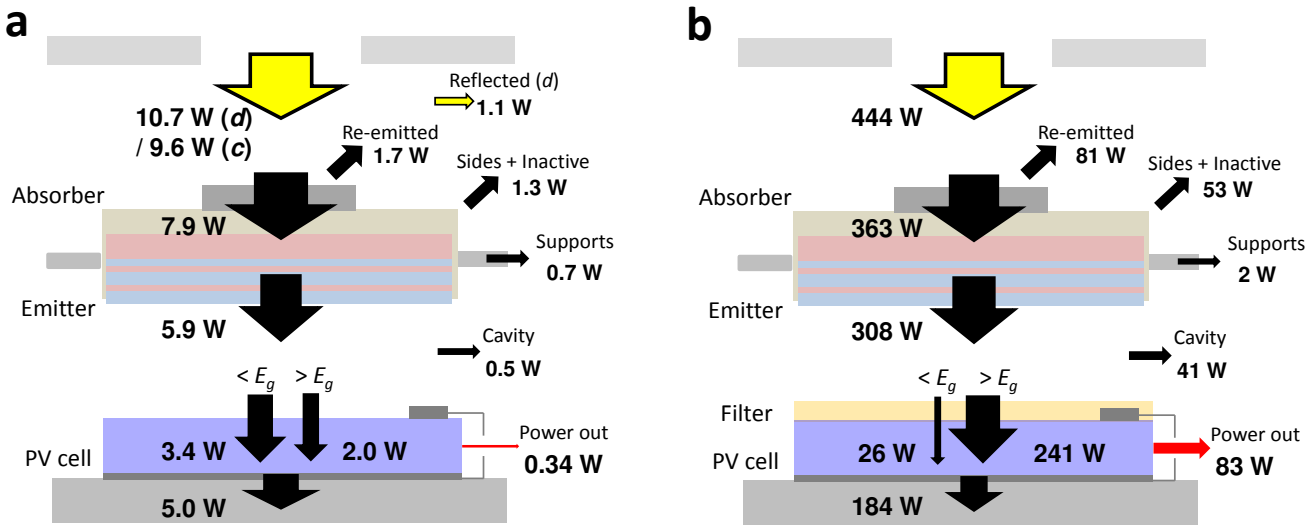

Supplementary Fig. 5 | Power conversion and loss mechanisms at an irradiance of 75 W/cm^2 in the following NARO-STPVs (obtained using the SQ1DD model): a, the experimentally demonstrated *AR*=7 (1cm^2) device (*d* and *c* represent diffuse and collimated irradiance, respectively); and **b,** a scaled-up (100 cm^2) *AR*=17 device utilizing a high-quality 0.55 eV PV module with a sub-bandgap reflector[6].The scaled-up device was simulated with 1 mm gaps between the shield/absorber and emitter/PV, and mounted using 8 stainless steel supports (difference between the diffuse and collimated irradiance is negligible in this configuration). Width of arrow is proportional to the magnitude of power it represents.

DOI: 10.1038/nnano.2013.286
SOURCE: Lenert, Andrej, David M. Bierman, Youngsuk Nam, Walker R. Chan, Ivan Celanović, Marin Soljačić, and Evelyn N. Wang. "A Nanophotonic Solar Thermophotovoltaic Device." Nature Nanotechnology 9, no. 2, p. 126–130, 2014.

References

1 Z.-P. Yang, L. Ci, J.A. Bur, S.-Y. Lin & P.M. Ajayan. Experimental observation of an extremely dark material made by a low-density nanotube array. *Nano Lett.* **8**, 446-451, (2008).
2 Z.-P. Yang *et al.* Experimental observation of extremely weak optical scattering from an interlocking carbon nanotube array. *Appl. Opt.* **50**, 1850-1855, (2011).
3 H. Shi, J.G. Ok, H.W. Baac & L.J. Guo. Low density carbon nanotube forest as an index-matched and near perfect absorption coating. *Appl. Phys. Lett.* **99**, 211103-211106, (2011).
4 Y. Nam *et al.* Solar thermophotovoltaic energy conversion systems with tantalum photonic crystal absorbers and emitters. *17th International Conference on Solid-State Sensors, Actuators and Microsystems.*(June 16-20, 2013, Barcelona, Spain)
5 W. Chan *et al.* Modeling low-bandgap thermophotovoltaic diodes for high-efficiency portable power generators. *Sol. Energ. Mat. Sol. C.* **94**, 509-514, (2010).
6 M.W. Dashiell *et al.* Quaternary InGaAsSb thermophotovoltaic diodes. *IEEE Trans. Electron.* **53**, 2879-2891, (2006).